Materials Advances

ROYAL SOCIETY OF CHEMISTRY

PAPER

View Article Online
View Journal | View Issue

Cite this: *Mater. Adv.*, 2023, 4, 3645

Mechanochromic, thermoresponsive and triboluminescence behaviors of one divinyl thioxanthene based AIE luminogen with variable conformations†

Nengni Xu,‡[a] Wenhua Xu,‡[a] Meng Sun,[b] Yi Yuan,[a] Xinjun Luan,*[a] Ying Wang[c] and Hui Wang*[a]

Strategic structure designs to develop organic multi-stimuli-responsive fluorescent materials are highly desired, but hard to achieve. We report here a novel multi-stimuli responsive luminescent material TXENE (1,2-di(9*H*-thioxanthen-9-ylidene)ethane) composed of double thioxanthene chromophores and a diene liker that integrate polymorphism, aggregation-induced emission (AIE), mechanoluminescence (MCL), thermoresponsive luminescence (TCL), and triboluminescent (TL) properties into one single molecule. Three crystalline polymorphs including TXENE-G and TXENE-Y with a terminal *up–down* conformer and TXENE-R with an *up–up* form are obtained. The X-ray structure analysis revealed that not only the intermolecular interactions but also the terminal chromophore-thioxanthene conformation (*up–down vs. up–up*) dominate polymorphism, thus leading to distinct luminescent properties. It is shown that MCL, TCL and TL properties can be systematically tuned *via* its aggregation state regulation; typically, the metastable TXENE-G and TXENE-R are MCL and TCL active, while TXENE-Y is TL active. Lastly, we illustrate the possible application of color-changeable indicators for information anti-counterfeiting and thermal sensing by using TXENE. This study demonstrates that multiple unique functions can be integrated into one single compound by fine controlling its aggregation states, which render a new strategy for the investigation of multifunctional organic materials.

Received 16th May 2023,
Accepted 12th July 2023

DOI: 10.1039/d3ma00239j

rsc.li/materials-advances

Introduction

As the society's dependence on technology continues to grow, the development of novel smart materials becomes increasingly important. Stimuli-responsive luminescent materials that demonstrate distinct emission character upon external stimuli have received great attention over the past few decades for their potent application in mechanosensors, security papers, and optical storage.[1–4] These chromic materials can be classified based on the types of external stimuli that they are responsive to. Mechanochromic materials[5,6] manifest variation of emission in the presence of mechanical stimuli, including shearing, grinding or rubbing as a result of the change in molecular packing between metastable and stable states. Thermally responsive materials refer to molecules that undergo molecular conformation, crystal structure or chemical reaction changes in response to temperature variations.[7,8] To date, a tremendous number of responsive materials have been reported focusing on the emission wavelength change;[9–11] however, the luminescence off and on response signal is also indispensable to realize optically activated dynamic materials. Triboluminescence (TL) is an interesting phenomenon of luminescence when certain solids are subjected to mechanical forces, which provides an effective complement for traditional photoexcitation or electroluminescence requiring UV irradiation or electrical excitation and shows potential utilization in smart optoelectronic devices.[12] We envisioned the possibility of integrating triboluminescence, mechanochromic and thermochromic properties into one-single molecule to build a multi-functional responsive material to realize versatile sensing of external environments.

Thanks to the innovative idea of aggregation-induced emission (AIE), the notorious luminescence quenching issue in

[a] *Key Laboratory of Synthetic and Natural Functional Molecule of the Ministry of Education, College of Chemistry & Materials Science, Northwest University, Xi'an, 710127, China. E-mail: whui210@nwu.edu.cn, xluan@nwu.edu.cn*
[b] *Key Laboratory of Molecular Medicine and Biotherapy, School of Life Sciences, Beijing Institute of Technology, Beijing 100811, China*
[c] *Key Laboratory of Photochemical Conversion and Optoelectronic Materials, Technical Institute of Physics and Chemistry, Chinese Academy of Sciences, Beijing, 100190, China*

† Electronic supplementary information (ESI) available. CCDC 2256584–2256586. For ESI and crystallographic data in CIF or other electronic format see DOI: https://doi.org/10.1039/d3ma00239j

‡ These authors contributed equally to this work.

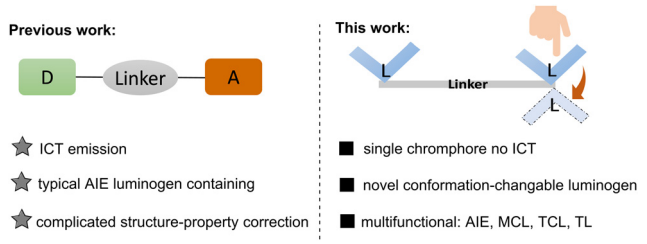

Scheme 1 The molecular design of TXENE and the comparison with previous work.

condensed states can be perfectly resolved, which guarantee high emission efficiency for solid stimuli-responsive materials.[13] The universal molecular design principle for mechanochromic materials include introduction of typical AIE moieties tetraphenyl ethylene (TPE)[14] or twisted triphenylamine (TPA)[15] structure into the donor–acceptor (D–A) scaffold to generate multiple non-covalent interactions (Scheme 1). Especially, the existence of locally excited (LE) and twisted intramolecular charge-transfer (TICT) states of D–A molecules diversified the optical properties; however, the latter are easily affected by steric substituents, conformation, D–A strength, and polarity environments, rendering the structure–property correction complicated.[16] Moreover, the head-to-tail densely packed arrangement caused by the oppositely charged electron density in the D–A skeleton may suppress the possibility of movement for specific moiety to produce metastable states, and thus inhibits the mechanochromism to some extent.[17,18] To this end, the exploration of simple and single chromic strategy for stimuli-responsive material design becomes an attractive complement.

The introduction of a conformation variable moiety into chromophores is an efficient strategy to design dynamic materials, which may generate multiple thermodynamically metastable states through conformational change under external stimuli.[19–21] In fact, a variety of smart luminescent materials have been achieved by Minakata,[22] Li[23] and Xu[24] by virtue of saddle-shaped phenothiazine building blocks bearing two distinct *quasi*-axial and *quasi*-equatorial conformers. However, conformation flexible chromophores are still limited and underdeveloped. Herein, we present a multi-stimuli-responsive material TXENE with mechanoresponsive, thermoresponsive and triboluminescent properties, which is composed of two butterfly-shaped thioxanthene units liked by rigid and conjugated dienes (Scheme 1). Importantly, TXENE can display two distinct *up–up* and *up–down* conformations based on the relative orientation of the butterfly-shaped thioxanthene, thus leading to different aggregated behaviours and luminescent properties.

Experimental methods

Materials and methods

Chemicals and reagents. Unless otherwise mentioned, all reagents were obtained from commercial sources such as Sigma-Aldrich, Innochem, *etc.* and used as received without any further purification. THF was dried over sodium and benzophenone was used as an indicator. The other reagents such as cyclopentyl methyl ether (CPME), HCl, ethanol, and acetic acid were purchased from Aladdin. All reactions were carried out under an argon atmosphere using standard Schlenk lines or a glovebox. Analytical thin-layer chromatography was performed with 0.25 mm coated commercial silica gel plates (TLC Silica Gel 60 F_{254}). Visualization of the developed chromatogram was performed by fluorescence. Flash chromatography was performed with silica gel (300–400 mesh).

Synthesis of 9-Methylene-9*H*-thioxanthene (1). To a round-bottomed flask (25 mL), thioxanthen-9-one (424.1 mg, 2 mmol) was charged under air. After the flask was evacuated and purged with nitrogen for three times, anhydrous THF (10.0 mL) was added using a syringe. Then 3 M (1 mL, 3 mmol) of methyl magnesium bromide in THF was added. The resulting mixture was stirred and refluxed for 16 h. After cooling, the organic phase was washed with 1 M HCl three times. The solvent was evaporated under reduced pressure to give an oil. To this oily residue, 2 M HCl (2 mL) was added and stirred until 9-methylene-9*H*-thioxanthene was completely consumed. It was extracted with saturated aq. $NaHCO_3$ and ethyl acetate three times. The organic phase was dried with anhydrous Na_2SO_4 and the solvent was removed under reduced pressure. The crude product was purified by flash silica gel column chromatography (petroleum ether/ethyl acetate = 100 : 1) to afford the desired product as colourless, air-sensitive oil.[25] (331.9 mg, 79% yield). ^{1}H NMR (400 MHz, chloroform-d) δ 7.85–7.75 (m, 2H), 7.62–7.53 (m, 2H), 7.47–7.36 (m, 4H), 5.75 (s, 2H). ^{13}C NMR (101 MHz, chloroform-d) δ 142.5, 134.7, 131.4, 128.0, 127.0, 126.3, 126.1, 114.0.

Synthesis of 9-(bromomethylene)-9*H*-thioxanthene (2). To a suspension of 1 (210.1 mg, 1 mmol) in AcOH (5 mL) was added NBS (178.0 mg, 1.1 mmol). The resulting mixture was stirred at 70 °C for 4 h. After cooling down to room temperature naturally, the reaction was neutralized by slowly adding NaOH/$NaHCO_3$ (1 : 1) and the mixture was extracted with ethyl acetate three times. The combined organic layers were dried over $MgSO_4$ and concentrated under reduced pressure. The residue was purified by silica gel flash chromatography (eluent : petroleum ether/ethyl acetate =100 : 1) to afford the desired product as a colorless oil.[26] (247.6 mg, 86% yield). ^{1}H NMR (400 MHz, chloroform-*d*) δ 8.06 (dd, J = 7.5, 1.8 Hz, 1H), 7.54 (dd, J = 7.5, 1.6 Hz, 1H), 7.48 (ddd, J = 9.1, 5.7, 3.0 Hz, 2H), 7.42–7.30 (m, 4H), 6.74 (s, 1H). ^{13}C NMR (101 MHz, chloroform-*d*) δ 139.4, 135.9, 133.2, 132.0, 131.8, 129.2, 128.0, 127.7, 127.0, 126.7, 126.0, 125.8, 125.8, 106.3.

Synthesis of 1,2-di(9*H*-thioxanthen-9-ylidene)ethane (TXENE). In a glovebox, a 5 mL vial equipped with a stirring bar was charged with 2 (57.6 mg, 0.2 mmol,), $PdCl_2$ (3.5 mg, 0.02 mmol), tris(4-methoxyphenyl) phosphine (14.1 mg, 0.04 mmol), and cesium carbonate (130.3 mg, 0.4 mmol) followed by the sequential addition of 2.0 mL anhydrous CPME. The vial was sealed with a Teflon screw cap and the reaction mixture was heated at 140 °C for 12 h. After this, the reaction vessel was cooled to room temperature. It was diluted with water and the reaction mixture was extracted with saturated aq. $NaHCO_3$ and ethyl acetate three

times. The organic phase was dried using anhydrous Na_2SO_4 and the solvent was removed under reduced pressure. The crude product was purified by flash silica gel column chromatography (petroleum ether) to afford the desired product as a yellow solid. (74.4 mg, 89% yield). ^{1}H NMR (400 MHz, chloroform-d) δ 7.83 (dd, J = 7.7, 1.4 Hz, 2H), 7.56 (dd, J = 7.7, 1.5 Hz, 2H), 7.52 (dd, J = 7.8, 1.4 Hz, 2H), 7.47–7.38 (m, 4H), 7.37–7.31 (m, 2H), 7.31–7.27 (m, 2H), 7.23 (td, J = 7.5, 1.5 Hz, 2H), 7.07 (s, 2H). ^{13}C NMR (101 MHz, chloroform-d) δ 137.9, 137.6, 133.7, 133.5, 131.8, 129.8, 127.8, 127.0, 127.0, 126.9, 126.7, 126.0, 125.9, 125.3. All ^{1}H NMR and ^{13}C NMR spectra are presented in the ESI.†

The conformation of structure. Proton nuclear magnetic resonance (^{1}H NMR) data were acquired on a Bruker Ascend 400 (400 MHz) spectrometer in $CDCl_3$ solutions, using tetramethylsilane (TMS) as an internal standard (δ = 0.00 ppm). Carbon-13 nuclear magnetic resonance (^{13}C NMR) data were acquired at 100 MHz on a Bruker Ascend 400 spectrometer using $CDCl_3$ as a solvent with chemical shift (δ = 77.16 ppm). High resolution mass spectra were acquired on a Bruker Daltonics MicroTof-Q II mass spectrometer in ESI mode.

The measurement of steady-state absorption and fluorescence. The UV-visible absorption spectra were determined on a Hitachi U-3310 spectrophotometer. Photoluminescence spectra were obtained using a Hitachi F-4600 fluorescence spectrophotometer. The TL spectrum was collected from a Hitachi F-4600 fluorescence spectrophotometer by concealing the source of excitation light and continuously grinding the compounds at the same time. The transient photoluminance decay and quantum yields (Φ_F) were determined using an Edinburgh FLS-920 with an integrating sphere. The DSC measurements were carried out using a TA Instruments DSC 2910 thermal analyzer at a heating rate of 2 °C min^{-1}.

The images of a confocal laser scanning microscope and a scanning electronic microscope. The images of a confocal laser scanning microscope (CLSM) were acquired using a Nikon-Sim laser microscope. The preparation of sample was carried out by dissolving TXENE in acetonitrile and water mixture with different water contents (20%, 40%, 60%, and 80%,). Morphologies of TXENE were observed using a scanning electronic microscope (SEM, CamScan Apollo 300) and analysed on cross-sectional SEM images using ImageJ software.

Powder X-ray diffraction measurement. The powder X-ray diffraction patterns (PXRD) were performed on a SHIMADZU XRD-600 Labx diffractometer with Cu-Ka radiation (λ = 1.5418 Å) at the 2θ range of 2–50°, 40 KeV, and 30 mA having a scanning rate of 0.01° s^{-1} (2θ) at room temperature.

Single-crystal X-ray diffraction measurement. The single-crystal X-ray diffraction was detected using a diffractometer equipped with a graphite monochromated Mo Kα (λ = 0.71073 Å, at 296(2) K) or a Bruker D8 venture photon II diffractometer with a graphite monochromated Ga Kα (λ = 1.34138 Å, at 150(2) K) radiation. The structure was solved with direct methods using SHELXTL programs and refined with full-matrix least squares on F^2. The corresponding CCDC reference number of CCDC 2256586† for TXENE-G, CCDC 2256585† for TXENE-Y, and CCDC 2256584† for TXENE-R, and the data can be obtained from the Cambridge Crystallographic Data Centre.

Theoretical calculation details. Density functional theory (DFT) calculations are performed using the Gaussian 09 program package. Molecular models are selected from the single crystal structures. Molecular structures of TXENE monomers at the ground state are optimized at the density functional B3LYP/6-31G (d) level. The excitation energies in singlet and triplet states are obtained using the time-dependent density functional theory (TD-DFT) method based on the optimized molecular structures at the ground state. (Hydrogens are omitted for clarity.)

Results and discussion

Design and synthesis

The target compound TXENE was synthesized through a facile and easy-to-handle three-step reaction, as shown in Scheme 2. First, thioxanthone and methyl magnesium bromide underwent a Witting reaction to generate 9-methylene-9*H*-thioxanthene **1** in 79% yield. Treatment of compound **1** with NBS in acetic acid afforded brominated thioxanthene **2** in 86% yield. Finally, the transition-metal catalysed homocoupling of compound **2** allowed the production of 1,2-di(9*H*-thioxanthen-9-ylidene)-ethane (TXENE) with 89% isolated yield. It was noteworthy that the final homocoupling is the result of numerous optimizations by trial and error, which provide a novel and additive-free route for palladium-catalysed Ullmann reaction[27,28] to facilitate the homocoupling of aryl halide instead of dehalogenation.

Photophysical properties

The steady-state UV-vis absorption and photoluminescence (PL) spectra of TXENE in different solutions are shown in Fig. S1 (ESI†). TXENE exhibits three major absorption peaks. The two bands at 249 and 312 nm are attributed to n–π* and π–π* transitions, respectively, which are characteristic of thioxanthene derivatives.[29] TXENE has extended conjugation extending the absorption characteristics to a longer wavelength (395 nm), as has previously been observed with other thioxanthone derivatives.[30] TXENE exhibits faint PL in solution with a blue-greenish emission color centered at 510 nm.

As shown in Fig. S1 (ESI†), changing the polarity of the solvents does not lead to the shift of absorption and emission wavelengths, indicating the likely exclusion of the presence of intramolecular charge transfer for their ground state or excited

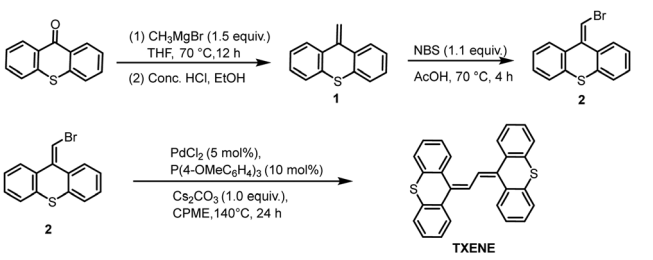

Scheme 2 Synthetic route to TXENE.

state. This result corresponds well with the absence of characteristic electron donors or acceptors in TXENE with a double thioxanthene-linked scaffold. In addition, TXENE does not give out light when molecularly dissolved in other solvents, such as toluene, CH_2Cl_2, THF or CH_3CN, as suggested by the low absolute photoluminescence quantum yields (PLQY) shown in Table S1 (ESI†).

In the diene linked fused aromatic system, the double bond was inclined to adopt the *trans*-configuration making the TXENE molecule arrange staggered in space. Taking the striction of intramolecular motion mechanism for AIE materials into consideration, we examined the AIE behavior of TXENE in acetonitrile/water mixtures following a literature method.[31] By mixing acetonitrile and water with different water contents, we observed a change in the trend of emission spectra with a quantitative change of the water content (Fig. 1(a) and (b)). The spectral intensity of TXENE reached the maximum and the PLQY enhanced by 208-fold, when the water fraction went up to 80%, indicating that molecular aggregates in this composition have the highest emission efficiency and TXENE is undoubtedly AIE-active. Interestingly, we observed an abnormal phenomenon that not only the PL intensity but also the emission wavelength changes with a quantitative change of water content, which are totally different for most traditional AIE molecules.[32–34] Due to the disappearance of the ICT effect in TXENE, we excluded the influence of electronic effect caused by solvent polarity on its emission spectra, and we speculate the possible interference of aggregate morphology on their emission properties. To this end, the micromorphology of aggregates under different water proportions was analysed by confocal laser scanning microscopy. As shown in Fig. 1(c)–(f), the micromorphologies of aggregates are completely different under distinct water ratios. At 20% water content, the aggregates demonstrate a dispersed, orderly crystalline particles with green fluorescence; it changed to dense square microcrystals doped with some floccules by 40% and emitted yellow light; at 60%, the aggregate morphology changes greatly and becomes a rod-like microcrystal. By 80%, it almost changed into a neat, rod-like crystal. In this regard, we speculated that the complexity and the coexistence of various microcrystalline morphologies are the main reasons that multiple emissive peaks exist in different mixtures as shown in Fig. 1(a). Therefore, it is essential to detect the polymorphism-dependent luminescence[35–37] properties of TXENE to better understand their photoluminescence in solid states and regulate their emission through self-assemble modulation.

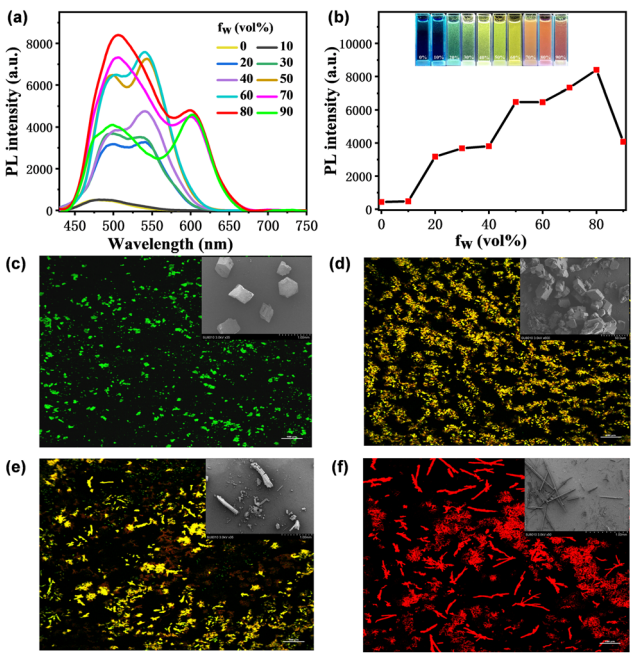

Fig. 1 (a) The photoluminescence of TXENE with increasing water fraction in a $CH_3CN:H_2O$ mixture (5×10^{-5} M); (b) plot of PL intensity *versus* the composition of CH_3CN/H_2O mixtures; confocal images with different water contents of 20% (c); 40% (d); 60% (e); and 80% (f).

Polymorphologies

To verify the above speculation, various solvents have been explored for growing crystals. Fortunately, three crystals that emits green (TXENE-G, rhombus-shaped crystal), yellow (TXENE-Y, flake-like crystal) and red (TXENE-R, rod-like crystal) fluorescence were produced by slow evaporation from *n*-hexane/CH_2Cl_2 (1 : 2), CH_2Cl_2 and CH_2Cl_2/CH_3OH (1 : 1) solutions, respectively (Table S2, ESI†). As shown in Fig. 2, TXENE-G and TXENE-Y crystals emit at 495 and 537 nm with PLQYs of 15.4% and 29.5%, respectively, while TXENE-R possesses a relatively weak red emission at 602 nm with a PLQY of 8.12%.

To further study their molecular conformation and packing mode, the single crystal structures of TXENE-G, TXENE-Y and TXENE-R were measured by single-crystal X-ray diffraction (XRD). As shown in Fig. 3, two butterfly-shaped thioxanthene moieties at each end of the rigid diene adopted distinct configurations: up and down direction (*up–down*) for TXENE-G and TXENE-Y, while uniformly upward (*up–up*) for TXENE-R. Different orientations of molecule make the crystal display an entirely different packing mode: the crystalline phase of TXENE-G and TXENE-Y is monoclinic with a space group of $P2_{1/c}$, whereas TXENE-R is triclinic with a space group of $P\bar{1}$. In TXENE-G, the molecules arrange in a complicated herringbone packing as seen from the *c*-axial (Fig. 3a), when considering every single molecule as a separated vector with certain direction. The molecule at each apex arranged cross-parallel to its adjacent molecule. Two adjacent thioxanthene rings overlap by every benzene-containing-half at a degree of approximately 40%

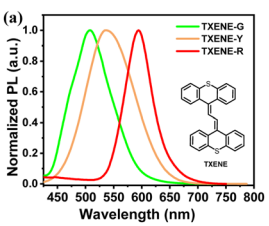

Crystal	Wavelength (nm)	PLQY (%)	Lifetime (ns)
TXENE-G	495	15.4	0.88
TXENE-Y	537	29.5	1.78
TXENE-R	602	8.12	1.52

Fig. 2 (a) PL spectra of TXENE in different aggregation states; (b) table summary of TXENE photoluminescence in three crystals.

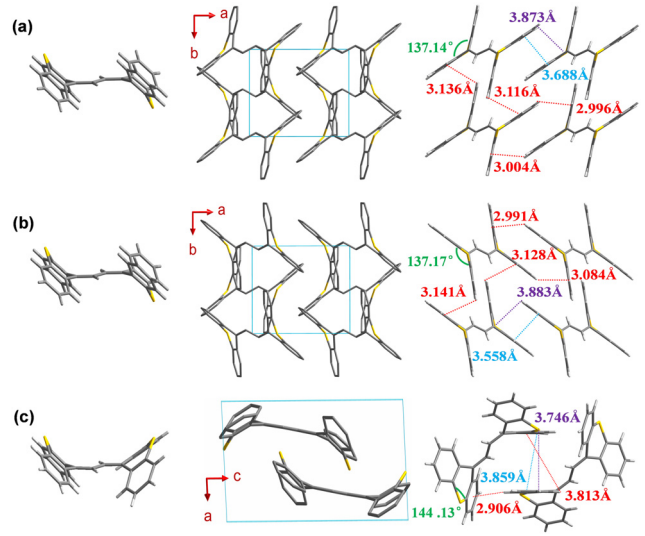

Fig. 3 Molecular conformation, crystal stacking mode and intermolecular interactions for TXENE-G (a); TXENE-Y (b); and TXENE-R (c) (inset: Red for CH–π, blue for π–π, and purple for CH–S interactions).

with centroid–centroid distances of 3.688 Å. Moreover, each molecule interacts with neighbouring molecules *via* four kinds of CH–π interactions and one kind of CH–S interaction, as shown in Fig. 3a top, with distances of 3.136 Å and 3.116 Å along the *a*-axial, 2.996 Å and 3.004 Å along the *b*-axial for CH–π interactions, and 3.873 Å for the CH–S interaction. Notably, the relatively weak π–π stacking and blades of the thioxanthene unit may help to produce metastable states under an external force, which may lead to mechanochromism. For TXENE-Y, there are no obvious differences between TXENE-G and –Y; however, careful measurements show that the dihedral angle of single thioxanthene for TXENE-Y was 137.17° (larger than 137.14° for TXENE-G), leading to much tighter arrangement. For example, π–π interaction between two centroids of adjacent thioxanthene changed from 3.688 Å to 3.558 Å. At this end, TXENE-Y can be considered as a stable assemble of metastable TXENE-G. Moreover, six intense intermolecular forces including CH–π, π–π and CH–S interactions, will be beneficial to fixing the molecular conformations and inhibiting intramolecular rotation,[38,39] which can explain the largest PLQY observed in TXENE-Y. In TXENE-R, TXENE form a tight dimer in which two thioxanthene rings are parallel on a head-to-tail arrangement in opposite sides. The top molecule combined with the below one through π–π interactions with distance of 3.859 Å, CH–π interactions with distances of 2.906 Å and 3.813 Å and CH–S interaction of 3.746 Å. Due to the relatively sparse arrangement and "the energy gap law"[40,41] for red emitter, the TXENE-R exhibits the lowest PLQY among the three polymorphs.

To unlock the underlying reasons for the different emission colours between TXENE-G and TXENE-Y, we focus on the aggregation pattern of crystals. Based on the absorption spectrum and crystalline analysis, we found that TXENE-G and TXENE-Y adopt distinct J-aggregation, while TXENE-R adopted tight dimer aggregation. First, we measured the absorption spectrum of the three polymorphs (Fig. S1d in ESI†). All three forms generate a moderate red-shift in the absorption spectrum compared to their solution counterparts, which are characteristic for J-aggregates. Second, as shown in Fig. 3, the single crystals of TXENE-G and TXENE-Y exactly show a similar molecular packing. However, the cell parameters and the bond length and dihedral angle of each molecule are still slightly different, including cell lengths of *a* 9.805(3), *b* 7.752(2), *c* 13.324(3) and cell angels of α 90, β 99.924(8), γ 90 for TXENE-G and cell lengths of *a* 9.810(2), *b* 7.7548(18), *c* 13.337(3) and cell angels of α 90, β 99.872(7), γ 90 for TXENE-Y. These differences cause the two crystals to form distinct aggregates. As shown in Fig. 4, the TXENE molecules are arranged in a head-to-tail fashion to form slipped π-stacks along the *a* and *b* axials with the shortest perpendicular π–π interactions ($d_{\pi-\pi}$) along the *c* axial of 3.196 Å for the G-form and 1.360 Å for the Y form, respectively. The pitch angles between the molecular transition dipole and the π-stack direction are 24.50° for the G-form and 29.34° for the Y-form single crystal, respectively, verifying that J-aggregation did occur in both the two polymorphisms. The relatively large slip distance (dP) of 7.01 Å for the G-form single crystal and 2.78 Å for the

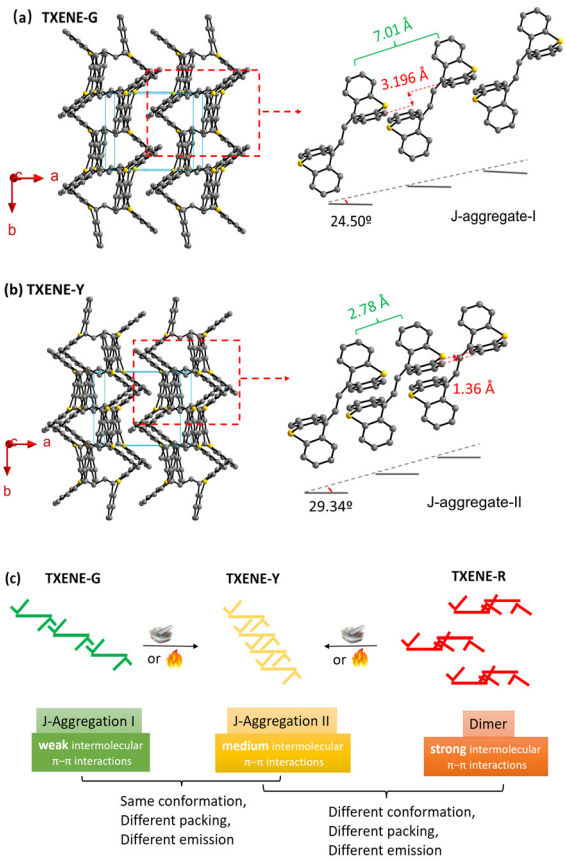

Fig. 4 The molecular arrangement top view of TXENE-G (a) and -Y (b) and three molecules view from approximately down the π-stacking axis, multicolor fluorescence of polymorphs through tuning the molecular packing (c).

Y-form single crystal along the *c* direction was measured. The reduced slip distance (2.78 *vs.* 7.01 Å) and reduced $d_{\pi-\pi}$ (1.36 *vs.* 3.19 Å) along the π-stacks, which would lead to the stronger intermolecular interactions between adjacent molecules, account for the red-shift of the emission from TXENE-G to TXENE-Y. In the case of TXENE-R, two single molecules form a pair of dimers in which half of one thioxanthene are parallel to each other, while another thioxanthene are on opposite sides (seen from Fig. 3c). It is worth noting that the benzene rings of parallel half thioxanthene overlap at a degree of approximately 96% with centroid–centroid distances of 3.859 Å between them, in which the vertical translation can almost been ignored. Such face-to-face π–π interactions in antiparallel dimers lead to the strongest intermolecular interactions between adjacent molecules compared to TXENE-G and -Y, accounting for the red emission of TXENE-R.

Mechanochromic and thermoresponsive luminescence

External mechanical force was applied to three polymorphs by grinding them using an agate mortar. No change was observed in TXENE-Y, indicating that TXENE-Y was composed of stable aggregates that resist external shearing. However, upon grinding TXENE-G, an obvious red-shifted emission from green to yellow was observed accompanying the PL wavelength change from 499 nm to double peak at 508 nm and 537 nm. Specifically, the new-appeared 537 nm of the ground solids were identical to those of the TXENE-Y crystal, implying that the external mechanical force may change the stacking pattern of the crystals resulting in a partially changed TXENE-G. Then PXRD was performed to understand the exact crystal transformation. As shown in Fig. 5d, the diffraction peaks almost overlapped each other between the simulated TXENE-Y and the ground TXENE-G except the weak and broad diffractions for the ground samples, revealing the disruption of the original crystal lattice of TXENE-G and the attainment of an amorphous state related to TXENE-Y.[42] The solvent DCM dissolution and recrystallization from DCM and methanol for the ground sample enables the reconstruction of the crystal lattice for TXENE-G to regain its original emission. On the other hand, the solid power generated from direct rotary evaporation of DCM presented an orange-red fluorescence with emission at 594 nm. The diffraction peaks of the orange solid are sharp and totally different from that of TXENE-Y, indicating that the orange solid more likely corresponds to the *up–up* conformer of TXENE-R. Upon grinding, it can enlighten the same yellow emission as TXENE-*G*-ground (centred at 508 and 537 nm), suggesting that the *up–up* metastable conformer can also change into the *up–down* stable conformer through mechanical stimulating.

In order to explore the thermoresponsive luminescence of TXENE, we heated the three crystals (heating rate 10 °C per minute) on a Linkam hot stage equipped with a fluorescence microscope. Upon heating, TXENE-G loses its fluorescence near the melting point; however, it regains a yellow fluorescence (537 nm) upon slight cooling. The difference in emission wavelength between TXENE-G and the cooled solid melt (TXENE-G-melt) is 38 nm, nearly in the same range as that observed upon grinding (Fig. 5c). TXENE-R displays the same phenomenon as TXENE-G, while, the stable TXENE-Y showed no significant change upon heating; this phenomenon can also be reflected by the absence of phase transition temperature in the DSC experiment (Fig. S4, ESI†). As a consequence, a comparatively weaker crystal packing of TXENE-G and TXENE-R plays an essential role in the excellent sensitivity against various external stimuli; both polymorphs eventually turn into the stable *up–down* conformer TXENE-Y upon shearing or heating.

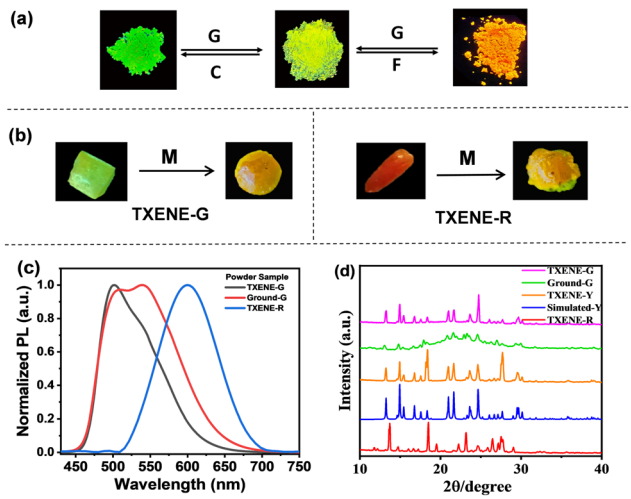

Fig. 5 Photographs of fluorescence under UV excitation (a) (G: grinding crushing; R: solving in DCM and recrystallization from methanol and DCM; C: solving in DCM and concentrating by rotary evaporation); (b) thermoresponsive behavior (H: heating to melt); PL spectra (c) and PXRD (d) for pristine TXENE-G, TXENE-R and their ground or heated variant.

Theoretical study

To rationalize the experimentally observed luminescence phenomenon, time-dependent density functional theory (TD-DFT) calculations were carried out to predict their HOMOs, LUMOs and conformational variation mechanism. The three model structures were extracted from the TXENE-G, TXENE-Y and TXENE-R crystals, respectively. As shown in Fig. 6, the HOMO and LUMO were spread over the whole molecule with slight difference on the diene linker due to the absence of characteristic electron donors or acceptors. Moreover, calculations of optical band gap using their crystal structure suggested the lowest band gap for TXENE-R and the highest for TXENE-G, which support their solid-state fluorescence. To disclose the conformational change upon the mechanical stimuli, we also simulated the transition states between TXENE-Y and TXENE-R. By setting up a series of minimizations, we found that the metastable TXENE-R with the *up–up* configuration can change into the stable TXENE-Y with the *up–down* configuration *via* one thioxanthene pseudoplanarization, which pass through an energy barrier of 10.6 kcal mol^{-1}. It is noteworthy that the conversion mechanism for TXENE conformers is ''inversion'', basically different from the excited-state ''rotation'' mechanism, in which the latter was reported to be the main mechanism for

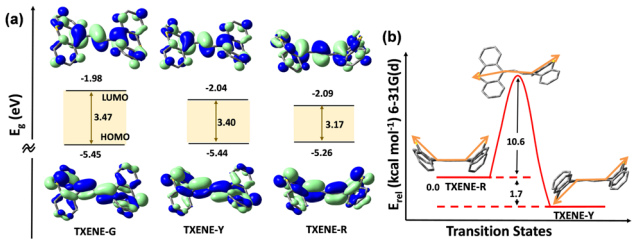

Fig. 6 (a) The calculated energy gaps (E_g) and HOMO–LUMO distribution for TXENE-G, -Y and -R; (b) calculated transition states for turning TXENE-R into -Y.

Feringa's molecular rotors[43] possessing an analogous molecular structure as TXENE.

Triboluminescence

By grinding the TXENE-Y crystals with a pestle, a faint yellow light emission centered at 550 nm was observed in the dark without UV irradiation. Remarkably, not only the TXENE-Y crystal had TL properties, TXENE-G and the prepared microcrystal powder also emitted apparent yellow light upon grinding with a spatula. However, the TXENE-R crystal was TL inactive. For this dynamic TL property, both G- and Y-isomers adopted a noncentrosymmetric space group in their crystals, which may create two opposite charge distributions across the crystal, producing an electric field that excites light when the crystal breaks.[44] The triboluminescence spectrum of TXENE-Y is shown in Fig. 7d, which overlapped well with its photoluminescence.

Applications in information anti-counterfeiting and environmental sensors

Given the reversible multi-stimuli responsive behavior of TXENE as the model materials presented above, we fabricated a simple "color-changing letter" device by placing black paper on a glass slide,[45] and the polymorphs TXENE was spread onto the vacant areas of the paper surface. As shown in Fig. 8a, the letters NWU, written using TXENE-G (letter "N"), TXENE-Y (letter "W") and TXENE-R (letter "U"), emitted three G–Y–R fluorescence and were expressed as the original state with input message of "000". Once someone exerted force on the letter "N", the letters emitted Y–Y–R, and this terminal state can be expressed as "100". Once the force was applied on the letter "U", the letters emitted G–Y–Y, and this terminal state can be

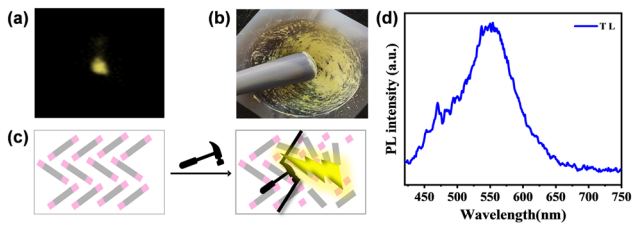

Fig. 7 TL images of TXENE powder in the dark (a) and under daylight (b) at room temperature; schematic diagram of the TL (c) and TL spectra of TXENE powder (d).

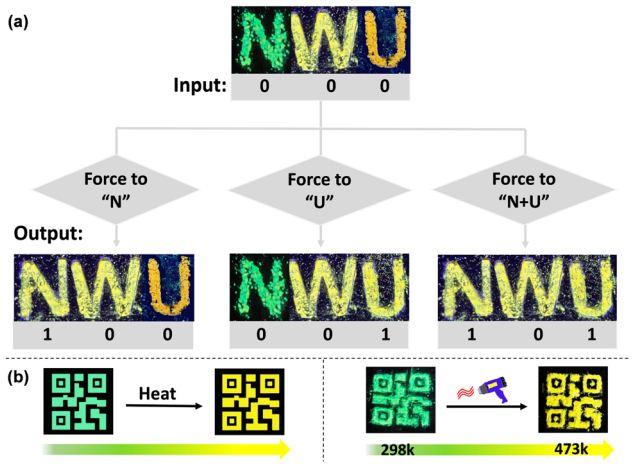

Fig. 8 (a) "Color-changing letter" device; (b) schematic representation (left) and photograph (right) of TXENE-G in visualized thermally imaging experiments (under 365 nm UV light).

expressed as "001". In a similar way, once the force was applied on "N + U", the letters emitted Y–Y–Y, and this terminal state can be expressed as "101". The fact that the forces applied at different locations show distinct luminescence can be used for simple information encryption or anti-counterfeit labeling.

Furthermore, the visualized thermally imaging experiment-induced PL switching is shown in Fig. 8b. At *RT*, the painted 2D code with TXENE-G presents a bright green emission under UV light. However, upon increasing the temperature, the color of the 2D code changed, red-shifted gradually and even became yellow as the temperature increased up to 473 K. This distinctive green-to-yellow thermoresponsiveness strongly suggests intrinsic molecular conformation and energy transfer from the metastable TXENE-G to the stable TXENE-Y, thus highlighting the potential application of TXENE in environmental sensors.

Conclusions

In summary, we have designed and synthesized a multi-stimuli-responsive luminescent material TXENE by the introduction of two flexible thioxanthene chromophores into the terminal of a diene linker. The emitter is AIE active and displays polymorphism-dependent luminescence properties. By carefully optimizing the recrystallization solvents, we succeeded in obtaining not only TXENE-G and TXENE-Y with *up–down* conformer but also TXENE-R with an *up–up* form. To our knowledge, this is the first demonstration of three polymorphisms for thioxanthene-conformer-based ethylene. Upon grinding and heating, the metastable TXENE-R and TXENE-G can transform into an amorphous state with analogous TXENE-Y packing, resulting in fluorescence modification from green to yellow to red. Further crystal analysis demonstrated that not only the intermolecular interactions but also the thioxanthene conformation (*up–down vs. up–up*) dominate the polymorphism and distinct mechanochromic properties. Through DFT-calculations, we

found a pseudoplanar transition state translate into ''inversion'' mechanism for mechanical induced transforming from TXENE-R to -Y. Additionally, a distinct triboluminescence phenomenon was obtained for TXENE-Y due to its distinct molecular packing and noncentrosymmetric space group. The outstanding mechanochromism, thermoresponsive and triboluminescence coupled with its AIE characteristic make it practical for application in the anti-counterfeit and environmental sensor fields. More importantly, the correlation between the packing mode in crystal and luminescent properties can provide guidance in the design of novel multifunctional organic solid materials.

Author contributions

N. Xu performed the experiment and analysed all data; W. Xu performed the theoretical calculation; M. Sun and Y. Yuan conducted the material application; X. Luan and Y. Wang provided technical or material support; and H. Wang wrote the paper and supervised the research.

Conflicts of interest

There are no conflicts to declare.

Acknowledgements

This work was supported by the National Science Foundation of China (202030065, 21925108), the Natural Science Basic Research Program of Shaanxi Province (2022JM-084), and the Tang Foundation of Northwest University (360151900004).

References

1 S. Yagai, S. Okamura, Y. Nakano, M. Yamauchi, K. Kishikawa, T. Karatsu, A. Kitamura, A. Ueno, D. Kuzuhara, H. Yamada, T. Seki and H. Ito, Design amphiphilic dipolar p-systems for stimuli-responsive luminescent materials using metastable states, *Nat. Commun.*, 2014, **5**, 4013–4023.
2 H. Sun, S. Liu, W. Lin, K. Zhang, W. Lv, X. Huang, F. Huo, H. Yang, G. Jenkins, Q. Zhao and W. Huang, Smart responsive phosphorescent materials for data recording and security protection, *Nat. Commun.*, 2014, **5**, 3601–3610.
3 V. Praveen, B. Vedhanarayanan, A. Mal, R. Mishra and A. Ajayaghosh, Self-assembled extended π-systems for sensing and security applications, *Acc. Chem. Res.*, 2020, **53**, 496–507.
4 L. Tu, Y. Xie, Z. Li and B. Tang, Aggregation-induced emission: Red and near-infrared organic light-emitting diodes, *SmartMat.*, 2021, **2**, 326–346.
5 Z. Chi, X. Zhang, B. Xu, X. Zhou, C. Ma, Y. Zhang, S. Liu and J. Xu, Recent advances in organic mechanofluorochromic materials, *Chem. Soc. Rev.*, 2012, **41**, 3878–3896.
6 C. Wang, B. Xu, M. Li, Z. Chi, Y. Xie, Q. Li and Z. Li, A stable tetraphenylethene derivative: Aggregation-induced emission, different crystalline polymorph, and totally different mechanoluminescent property, *Mater. Horiz.*, 2016, **3**, 220–225.
7 Y. Wu, X. Zhang, Y. Zhang, M. Yang and Z. Chen, Achievement of ligand-field induced thermochromic luminescence via two-step single-crystal to single-crystal transformations, *Chem. Commun.*, 2018, **54**, 13961–13964.
8 X. Luo, J. Li, C. Li, L. Heng, Y. Dong, Z. Liu, Z. Bo and B. Tang, Reversible switching of the emission of diphenyldibenzofulvenes by thermal and mechanical stimuli, *Adv. Mater.*, 2011, **23**, 3261–3265.
9 P. Theato, B. Sumerlin, R. O'Reilly and T. Epps, Stimuli responsive materials, *Chem. Soc. Rev.*, 2013, **42**, 7055–7056.
10 F. Nie, K.-Z. Wang and D. Yan, Supramolecular glasses with color-tunable circularly polarized afterglow through evaporation-induced self-assembly of chiral metal–organic complexes, *Nat. Commun.*, 2023, **14**, 1654–1667.
11 F. Nie and D. Yan, Macroscopic Assembly of Chiral Hydrogen-bonded Metal-free Supramolecular Glasses for Enhanced Color-tunable Ultralong Room Temperature Phosphorescence, *Angew. Chem. Int. Ed.*, 2023, e202302751.
12 C. Wang and Z. Li, Molecular conformation and packing: their critical roles in the emission performance of mechanochromic fluorescence materials, *Mater. Chem. Front.*, 2017, **1**, 2174–2194.
13 J. Luo, Z. Xie, J. Lam, L. Cheng, H. Chen, C. Qiu, H. Kwok, X. Zhan, Y. Liu, D. Zhu and B. Tang, Aggregation-induced emission of 1-methyl-1,2,3,4,5-pentaphenylsilole, *Chem. Commun.*, 2001, 1740–1741.
14 G. Huang, Y. Jiang, S. Yang, B. Li and B. Tang, Multistimuli response and polymorphism of a novel tetraphenylethylene derivative, *Adv. Funct. Mater.*, 2019, **29**, 1900516.
15 Z. Xie, T. Yu, J. Chen, E. Ubba, L. Wang, Z. Mao, T. Su, Y. Zhang, M. Aldred and Z. Chi, Weak interactions but potent effect: Tunable mechanoluminescence by adjusting intermolecular C-H...π interactions, *Chem. Sci.*, 2018, **9**, 5787–5794.
16 L. Zhan, Z. Chen, S. Gong, Y. Xiang, F. Ni, X. Zeng, G. Xie and C. Yang, A simple organic molecule realizing simultaneous TADF, RTP, AIE, and mechanoluminescence: Understanding the mechanism behind the multifunctional emitter, *Angew. Chem. Int. Ed.*, 2019, **58**, 17651–17655.
17 S. Park, S. Varghese, J. Kim, S.-J. Yoon, O. Kwon, B.-K. An, J. Gierschner and S. Park, Tailor-Made highly luminescent and ambipolar transporting organic mixed stacked charge-transfer crystals: An isometric donor-acceptor approach, *J. Am. Chem. Soc.*, 2013, **135**, 4757–4764.
18 B. Roy, M. Reddy and P. Hazra, Developing the structure-property relationship to design solid state multi-stimuli responsive materials and their potential applications in different fields, *Chem. Sci.*, 2018, **9**, 3592–3606.
19 W. Fu, T. Alam, J. Li, J. Bustamante, T. Lien, R. Adams, S. Teat, B. Stokes, W. Yang, Y. Liu and J. Lu, Arene substitution design for controlled conformational changes of dibenzocycloocta-1,5-dienes, *J. Am. Chem. Soc.*, 2020, **142**, 16651–16660.
20 Z.-F. Liu, X. Chen, Z. Mou and W. Jin, Stimuli-responsive luminescent bithiophene-dicarbaldehyde molecular rotors

by hydrogen bonding, *J. Mater. Chem. C*, 2020, **8**, 16100–16106.

21 J. Ren, Y. Wang, Y. Tian, Z. Liu, X. Xiao, J. Yang, M. Fang and Z. Li, Force-induced turn-on persistent roomtemperature phosphorescence in purely organic luminogen, *Angew. Chem. Int. Ed.*, 2021, **133**, 12443–12448.

22 M. Okazaki, Y. Takeda, P. Data, P. Pander, H. Higginbotham, A. Monkman and S. Minakata, Thermally activated delayed fluorescent phenothiazine-dibenzo[a,j]-phenazine-phenothiazine triads exhibiting tricolor-changing mechanochromic luminescence, *Chem. Sci.*, 2017, **8**, 2677–2686.

23 J. Yang, J. Qin, P. Geng, J. Wang, M. Fang and Z. Li, Molecular conformation-dependent mechanoluminescence: Same mechanical stimulusbut different emissive colorover time, *Angew. Chem. Int. Ed.*, 2018, **57**, 14174–14178.

24 Y. Chen, C. Xu, B. Xu, Z. Mao, J.-A. Li, Z. Yang, N. Peethani, C. Liu, G. Shi, F. Gu, Y. Zhang and Z. Chi, Chirality-activated mechanoluminescence from aggregation-induced emission enantiomers with high contrast mechanochromism and force-induced delayed fluorescence, *Mater. Chem. Front.*, 2019, **3**, 1800–1806.

25 T. Jepsen, M. Larsen, M. Jørgensen and M. Nielsen, Three-step synthesis of (thio)xanthene and dibenzothiepine/diben-zoxepine by an intramolecular Mizoroki–Heck reaction of diaryl (thio)Ethers, *Synlett*, 2012, 418–422.

26 G. Zhang, R. Bai, C. Li, C. Feng and G. Lin, Halogenation of 1,1-diarylethylenes by N-halosuccinimides, *Tetrahedron*, 2019, **75**, 1658–1662.

27 D. Hennings, T. Iwama and V. Rawal, Palladium-catalyzed (Ullmann-type) homocoupling of aryl halides: A convenient and general synthesis of symmetrical biaryls via inter-and intramolecular coupling reactions, *Org. Lett.*, 1999, **1**, 1205–1208.

28 M. Yu, R. Tang and J. Li, Synthesis of 6,7-dihydro-5H-dibenzo[c,e]azepines and biaryls by palladium-catalyzed Ullmann reaction, *Tetrahedron*, 2009, **65**, 3409–3416.

29 A. Marcinek, J. Rogowski, J. Adamus, J. Gebicki and M. Platz, Sequential electron-proton-electron transfer in the radiolytic and photochemical oxidation of thioxanthene and xanthene, *J. Phys. Chem.*, 1996, **100**, 13539–13543.

30 G. Yilmaz, B. Aydogan, G. Temel, N. Arsu, N. Moszner and Y. Yagci, Thioxanthone-fluorenes as visible light photoinitiators for free radical polymerization, *Macromolecules*, 2010, **43**, 4520–4526.

31 J. Mei, Y. Hong, J. Lam, A. Qin, Y. Tang and B. Tang, Aggregation-induced emission: The whole is more brilliant than the parts, *Adv. Mater.*, 2014, **26**, 5429–5479.

32 B. Xu, J. He, Y. Mu, Q. Zhu, S. Wu, Y. Wang, Y. Zhang, C. Jin, C. Lo, Z. Chi, A. Lien, S. Liu and J. Xu, Very bright mechanoluminescence and remarkable mechanochromism using a tetraphenylethene derivative with aggregation-induced emission, *Chem. Sci.*, 2015, **6**, 3236–3241.

33 G. Huang, Q. Xia, W. Huang, J. Tian, Z. He, B. Li and B. Tang, Multiple anti-counterfeiting guarantees from a simple tetraphenylethylene derivative-high-contrasted and multi-state mechanochromism and photochromism, *Angew. Chem. Int. Ed.*, 2019, **131**, 17978–17983.

34 J. Wang, J. Mei, R. Hu, J. Sun, A. Qin and B. Tang, Click synthesis, aggregation-induced emission, E/Z isomerization, self-organization, and multiple chromisms of pure stereoisomers of a tetraphenylethene-cored luminogen, *J. Am. Chem. Soc.*, 2012, **134**, 9956–9966.

35 S. Liu, Y. Lin and D. Yan, Hydrogen-bond organized 2D metal–organic microsheets: direct ultralong phosphorescence and color-tunable optical waveguides, *Sci. Bull.*, 2022, **67**, 2076–2084.

36 D. Yan and D. Evans, Molecular crystalline materials with tunable luminescent properties: from polymorphs to multi-component solids, *Mater. Horiz.*, 2014, **1**, 46–57.

37 Y.-J. Ma, G. Xiao, X. Fang, T. Chen and D. Yan, Leveraging crystalline and amorphous states of a metal-organic complex for transformation of the photosalient effect and positivenegative photochromism, *Angew. Chem. Int. Ed.*, 2023, **62**, e20221705.

38 Q. Qi, J. Qian, X. Tan, J. Zhang, L. Wang, B. Xu, B. Zou and W. Tian, Remarkable turn-on and color-tuned piezochromic luminescence: Mechanically switching intramolecular charge transfer in molecular crystals, *Adv. Funct. Mater.*, 2015, **25**, 4005–4010.

39 Y. Gong, P. Zhang, Y. Gu, J. Wang, M. Han, C. Chen, X. Zhan, Z. Xie, B. Zou, Q. Peng, Z. Chi and Z. Li, The influence of molecular packing on the emissive behavior of pyrene derivatives: Mechanoluminescence and mechanochromism, *Adv. Opt. Mater.*, 2018, **6**, 1800198.

40 J. Caspar, E. Kober, B. Sullivan and T. Meyer, Application of the energy gap law to the decay of charge-transfer excited states, *J. Am. Chem. Soc.*, 1982, **104**, 630–632.

41 Y. Zhang, D. Zhang, T. Huang, A. Gillett, Y. Liu, D. Hu, L. Cui, Z. Bin, G. Li, J. Wei and L. Duan, Multi-resonance deep-red emitters with shallow potential-energy surfaces to surpass energy-gap law, *Angew. Chem., Int. Ed.*, 2021, **60**, 20498–20503.

42 T. Seki and H. Ito, Molecular-level understanding of structural changes of organic crystals induced by macroscopic mechanical stimulation, *Chem. – Eur. J.*, 2016, **22**, 4322–4329.

43 G. Sánchez-Sanz, I. Alkorta and J. Elguero, Isomerization barriers in bis(4H-thiopyran) and in bithioxanthenes, *Tetrahedron*, 2011, **67**, 7316–7320.

44 Y. Xie and Z. Li, The development of mechanoluminescence from organic compounds: Breakthrough and deep insight, *Mater. Chem. Front.*, 2020, **4**, 317–331.

45 L. Ma, B. Ding, Z. Yuan, X. Ma and H. Tian, Triboluminescence and selective hydrogen-bond responsiveness of thiochromanone derivative, *ACS Mater. Lett.*, 2021, **3**, 1300–1306.